AGU
ADVANCING
EARTH AND
SPACE SCIENCE

Earth and Space Science

RESEARCH ARTICLE

Key Points:

- Cassini revealed a variety of organic compounds including clear evidence of aromatics in the plume of Enceladus
- Identifying mass spectral features of isomeric organics enhances our ability to assess the astrobiological potential of Enceladus/Europa
- Parent aromatic compounds can be easily distinguished from their derivatives in ice grains with impact ionization mass spectrometry

Supporting Information:

Supporting Information may be found in the online version of this article.

Correspondence to:

N. Khawaja,
nozair.khawaja@fu-berlin.de

Author Contributions:

Conceptualization: N. Khawaja
Formal analysis: N. Khawaja, T. R. O'Sullivan, J. Hillier
Investigation: N. Khawaja
Methodology: N. Khawaja, F. Klenner, J. Hillier
Project Administration: N. Khawaja
Visualization: N. Khawaja, L. H. Sanchez
Writing – original draft: N. Khawaja

Discriminating Aromatic Parent Compounds and Their Derivative Isomers in Ice Grains From Enceladus and Europa Using a Laboratory Analogue for Spaceborne Mass Spectrometers

N. Khawaja[1] , T. R. O'Sullivan[1,2] , F. Klenner[1] , L. H. Sanchez[1], and J. Hillier[1]

[1]Institute of Geological Sciences, Freie Universität Berlin, Berlin, Germany, [2]International Space University, Strasbourg Central Campus, Illkirch-Graffenstaden, France

Abstract Results from the Cassini-Huygens space mission at Enceladus revealed a substantial inventory of organic species embedded in plume and E ring ice grains originating from a global subsurface and putative habitable ocean. Compositional analysis by the Cosmic Dust Analyzer indicated the presence of aromatic species and constrained some structural features, although their exact nature remains unclear. As indicated by many studies, among other organic species, low-mass aromatics likely played a role in the emergence of life on Earth and may be linked to potential prebiotic or biogenic chemistry on icy moons. Here, we study the behavior of single-ringed aromatic compounds—benzoic acid and two isomeric derivatives, 2,3-dihydroxybenzoic acid and 2,5-dihydroxybenzoic acid—using Laser-Induced Liquid Beam Ion Desorption (LILBID), an analogue setup to simulate the impact ionization mass spectra of ice grains in space. These compounds share common structural features but also exhibit differences in functional groups and substituent positions. We investigate the fragmentation behavior and spectral appearance of each molecule over three simulated impact velocities, in both positive and negative ion modes. Parent compounds can be distinguished easily from their derivatives due to various spectral differences, including the (de)protonated molecular ion peaks appearing at different m/z values. We conclude that distinction between structural isomers in LILBID is more challenging, but some insights can be revealed by considering intermolecular bonding regimes. This work will guide future investigations into elucidating the composition of isomeric biosignatures in ice grains, relevant for future space missions to Enceladus and Europa.

Plain Language Summary The Cassini-Huygens space mission discovered a plume at Enceladus that ejects gases and frozen ice grains originating from an ocean of liquid water below its icy shell. In these ice grains, a range of interesting organic molecules were discovered by Cassini's Cosmic Dust Analyzer mass spectrometer. Organic molecules are important in the search for life beyond Earth as they form the basis of all known Earth life, and active biology elsewhere would likely have a discernible effect on the local inventory of organic species. One class of organic, with a ring structure of carbon atoms, called aromatics, were discovered in the plume. We investigate the spectral appearance of one example of aromatic compound, benzoic acid, as well as two similar compounds with additional chemical groups attached to the aromatic ring. The two similar compounds have the same mass and general structure, but slightly different arrangements of the additional groups, known as isomers. We find that it is simple to distinguish mass spectral features between benzoic acid and its related compounds, but more difficult to explain the differences between the isomers. This work will assist the analysis of mass spectrometry data from future habitability-investigating space missions to ocean-bearing icy moons.

1. Introduction

Mass spectrometers on space missions, e.g., Galileo, Stardust, Cassini-Huygens, and Rosetta, have demonstrated the applicability of mass spectrometry for the in situ analysis of dust and ice grains in different planetary environments (Kissel et al., 2003; Scherer et al., 2006; Srama et al., 2004; Thiessenhusen et al., 2000). The Cassini-Huygens mission investigated the Saturnian system—planet, rings, and moons—for 13 years between 2004 and 2017. The mission experienced significant successes with the Cosmic Dust Analyzer (CDA) and Ion and Neutral Mass Spectrometer (INMS) instruments (Srama et al., 2004; Waite et al., 2006), revealing unprecedented results related to Saturn's moon Enceladus (Schenk et al., 2018).

Writing – review & editing: T. R. O'Sullivan, F. Klenner, L. H. Sanchez

Enceladus is a small, cryovolcanically active moon that orbits Saturn within the densest part of the E ring. Beneath its icy crust, Enceladus harbors a global subsurface ocean of liquid water, supported by tidal heating, which is in contact with its rocky core (Hsu et al., 2015; Postberg et al., 2009). At this ocean-core interface, hydrothermal activity is strongly suspected to be ongoing, diversifying the chemical inventory in the depths of the Enceladean ocean (Hsu et al., 2015; Waite et al., 2017). A plume, consisting of many individual jets, expels subsurface material originating from the ocean from four parallel fractures, the so-called tiger stripes, located in the south polar terrain (Spencer et al., 2006). This plume is the source of E ring ice grains (Spahn et al., 2006) and was successfully sampled during the Cassini mission. Another plume of gas and ice grains may be present on the Jovian moon Europa, which also hosts a subsurface ocean and may experience seafloor hydrothermal activity (Hand et al., 2007; Jia et al., 2018; Roth et al., 2014; Sparks et al., 2016). The presence of a liquid water ocean and hydrothermal activity on these planetary bodies, combined with the easily accessible sampling environment presented by the plumes, makes them prime targets in the search for extraterrestrial life.

The Cassini mass spectrometers conducted measurements of both vapor-phase and solid-phase plume components at Enceladus and in the E ring. INMS was sensitive for the compositional analysis of gaseous species, while CDA analyzed dust and ice grains and is relevant for this work. CDA worked on the principle of impact ionization whereby micron and submicron sized ice and dust grains hit the rhodium metal target of the instrument at velocities ≥ 1 km/s. On impact, these particles were vaporized, ionized, and dispersed into impact clouds containing ions, electrons, neutrals, and macromolecular fragments. The cations generated upon impact were accelerated toward the mass analyzer, producing time-of-flight (TOF) mass spectra with resolutions $m/\Delta m \sim 20$–50 (Srama et al., 2004).

CDA experienced unprecedented success in sampling the plumes of Enceladus, revealing extensive compositional diversity in ice grains. The detection of silica (SiO_2) nanoparticles indicating ongoing alkaline hydrothermal activity at elevated temperatures ($\approx 90°C$) in the depths of the Enceladus ocean (Hsu et al., 2015), similar to the terrestrial Lost City hydrothermal field on the mid-Atlantic seafloor, has further revealed the ocean to be putatively habitable. Postberg et al. (2018) and Khawaja et al. (2019) reported the detection of high mass complex macromolecular (≥ 200 u) as well as low-mass semivolatile (≤ 100 u) aromatic, and nitrogen-bearing and oxygen-bearing organic compounds. These studies have indicated huge compositional and structural diversity in organic compounds originating from the depths of the Enceladus ocean. Besides oxygen-bearing and nitrogen-bearing functional groups and aliphatic hydrocarbon side chains, the structural properties of the plume organics also imply the presence of single-ringed or multiringed aromatic species.

In addition, the discovery of abiotic amino acids in the Lost City hydrothermal field on Earth—which hosts similar conditions (pH and temperature) to the hydrothermal vent systems on Enceladus—by Ménez et al. (2018) suggests that single-ringed aromatic structures may play a key role in synthetic pathways to biomolecules. The authors propose that Friedel-Crafts(-like) reactions may provide a route from aromatic hydrocarbons to proteinogenic aromatic amino acids, tryptophan in this case. The presence of applicable catalytic minerals and favorable thermodynamic conditions in Lost City raises the possibility of a pathway involving alkylation followed by reductive amination (Barge et al., 2019; Cody et al., 2000; Khawaja et al., 2019). As a result, single-ringed aromatic compounds could also potentially be involved in prebiotic or biogenic chemistry in Enceladean hydrothermal sites at or inside its rocky core. Therefore, it is of great importance to understand the exact composition and the structural properties of aromatic compounds in the ice grains originating from Enceladus', and Europa's tentative, subsurface oceans.

In this work, we investigate single-ringed aromatic acids—namely, benzoic acid (C_7H_6O), and two of its hydroxy derivatives—2,3-dihydroxybenzoic acid and 2,5-dihydroxybenzoic acid (DHBA; $C_7H_6O_4$). Figure 1 details the molecular structures of the DHBAs and benzoic acid. The work of Postberg et al. (2018) and Khawaja et al. (2019) revealed that the higher mass complex macromolecular fragments detected in the plumes are likely insoluble, inviting the possibility of a benzoic acid-like aromatic units due to its poor solubility in water. Furthermore, the high relative abundances of benzene-like cations highlighted by Khawaja et al. (2019) suggest the presence of phenyl and/or benzoyl-like aromatic compounds. Laboratory analogue investigations in the same work revealed the preference of phenyl cation formation when an aromatic ring is attached to a nonalkyl group.

Furthermore, aromatic carboxylic acids have been discovered in carbonaceous meteorites and are speculated to exist in low-temperature interstellar ices (McMurtry et al., 2016; Remusat et al., 2005). In particular, benzoic acid was identified in the Murchison and Orgueil meteorites (Martins et al., 2006). Benzoic acid is heavily involved in biosynthetic processes and often acts as an intermediate toward more complex molecules, such as amino acids and secondary metabolites (Cobb, 2014; Widhalm & Dudareva, 2015). 2,3-DHBA is found naturally in some plants, and acts as a metabolite in many forms of life, including humans (Grootveld & Halliwell, 1988; Li et al., 2014). 2.5-DHBA is also
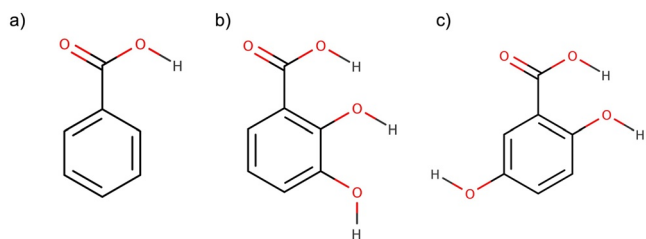
Figure 1. The molecular structures of (a) benzoic acid, (b) 2,3-DHBA and (c) 2,5-DHBA.

a metabolite and is present across a range of plant and animal species (Juurlink et al., 2014; Sankaranarayanan et al., 2019). Structural isomerism itself has also been suggested as a potential indicator of biotic processes, in combination with the search for enantiomeric excess and isotopic depletion (Glavin et al., 2020; Summons et al., 2008). Additionally, aromatic compounds, such as those studied in this work, and their complexes may form in hydrothermal systems like those present on Enceladus and potentially Europa, as well as on Earth and other icy moons (Venturi et al., 2017). Analysis of their mass spectral appearance continues to build toward a spectral reference library for space missions to the outer solar system (Klenner et al., 2022). The distinction of structural isomers by mass spectrometry is generally challenging. There are solutions offered, however, by utilizing a separation method prior to mass spectrometry in a laboratory setting (Reusch et al., 2018), although this is not feasible for spaceborne impact ionization instruments. In the same study, the authors find that isomers of other disubstituted benzene derivatives could be differentiated using chirped femtosecond laser ionization by ion yield ratios drawn from the mass spectra.

In this work, we use Laser-Induced Liquid Beam Ion Desorption (LILBID), a proven analogue technique that simulates impact ionization mass spectra of water ice grains in space, which has been crucial to the analysis of CDA mass spectra (Klenner et al., 2019). For the first time, we investigate the fragmentation behavior and spectral appearance of these aromatic acids (benzoic acid, 2,5-DHBA and 2,3-DHBA) and the influence of substituent functional groups on the mass spectra measured in both cationic and anionic modes with LILBID. We focus on fragmentation pathways of different structural isomers and compare them to discriminate their composition. Such comparisons may reveal key similarities or differences in the mass spectra that could be considered indicators of a certain isomer. Our work will not only assist in the interpretation of existing spacecraft data (e.g., Cassini's CDA), but will also provide guidance to upcoming space missions (NASA's Europa Clipper and JAXA's Destiny+) carrying CDA-like impact ionization mass spectrometers (SUrface Dust Analyzer—SUDA; Kempf et al., 2014 and Destiny Dust Analyzer—DDA; Krüger et al., 2019).

2. Methods

The LILBID facility utilized in this work is situated at the Freie Universität Berlin (FUB) in Germany and has been used to measure mass spectra of a variety of organic and inorganic compounds dissolved in water or other organic solvents (Charvat & Abel, 2007; Khawaja et al., 2019; Klenner, Postberg, Hillier, Khawaja, Cable, et al., 2020; Klenner, Postberg, Hillier, Khawaja, Reviol, et al., 2020). LILBID has also been used for astrobiology investigations to predict the spectral appearances and detection limits of biosignatures in impact ionization mass spectrometers (Dannenmann et al., 2022). Similar mechanisms are utilized in both LILBID and CDA-like spaceborne impact ionization mass spectrometers (Wiederschein et al., 2015). We present a brief introduction to the LILBID-TOF mass spectrometry process, with more detailed information available in Klenner et al. (2019). The setup for LILBID is detailed in Figure 2.

With the LILBID method, a beam of liquid solvent containing the dissolved analyte compound is vertically injected into a vacuum chamber ($\sim5 \times 10^{-5}$ mbar) through a quartz nozzle (radius ~ 7–12 µm) at a constant flow rate (typically ~0.2–0.35 mL min^{-1}; maintained by an HPLC pump). The liquid flow remains stable for ~2–3 mm downwards before forming droplets (Charvat & Abel, 2007). In the chamber, the liquid beam is intersected by a pulsed (20 Hz) infrared laser, which irradiates the beam with variable pulse energies of up to 4 mJ at a wavelength that matches the OH-stretch absorption frequency of water ($\sim2,850$ nm). The liquid beam absorbs the laser energy in a near-surface region which initiates the mechanical dispersion of both charged and neutral atomic, molecular, and macroscopic fragments (Charvat & Abel, 2007; Wiederschein et al., 2015). The energy absorbed by the system remains below the nominal ionization potentials and bond enthalpies of present species; the formation of ions is therefore believed to be governed by rapid changes in the charge density distribution within the matrix. This process almost exclusively creates singly charged cations and anions (Karas et al., 2000), which then pass through a field-free drift region, after which they are accelerated using the principle of delayed extraction and subsequently analyzed in a reflectron-type TOF mass spectrometer, with a mass resolution $m/\Delta m \sim 600$–800 and a mass range $m/z > 1,000$, far exceeding those of CDA (Srama et al., 2004). This TOF mass spectrometer is also a suitable analogue for SUDA, which will offer a mass range of up to m/z 500 and a mass resolution of 150–300 $m/\Delta m$
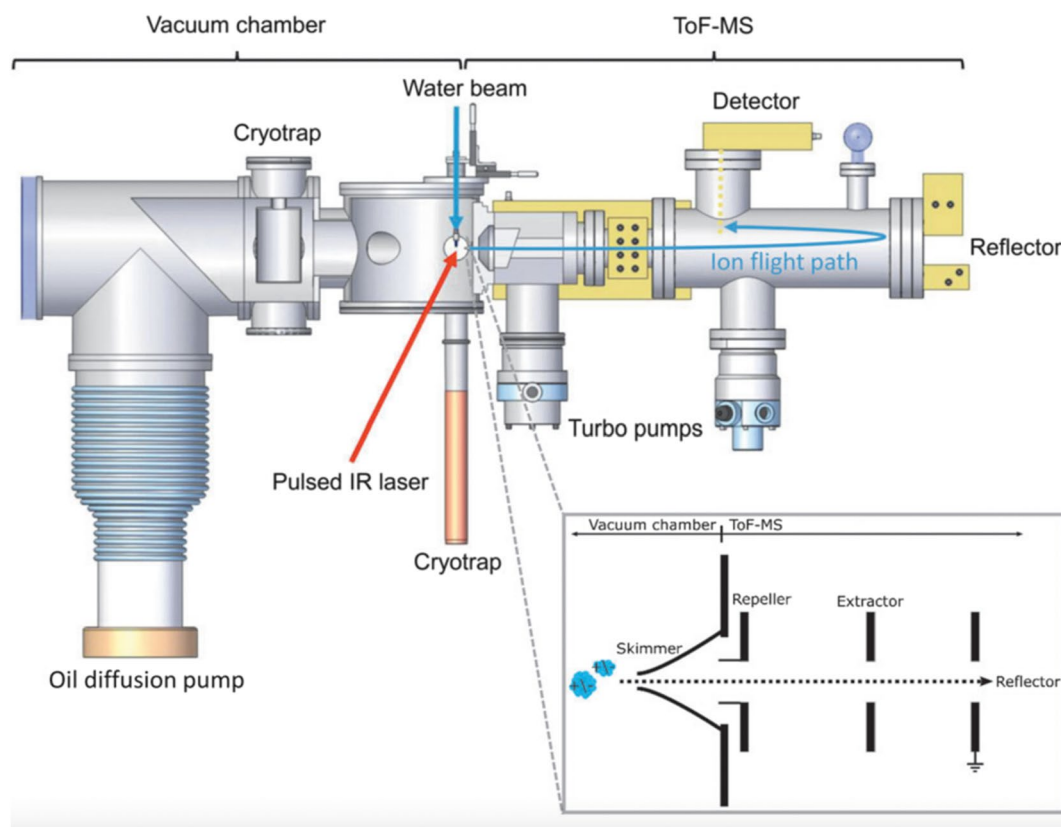
Figure 2. The Laser-Induced Liquid Beam Ion Desorption (LILBID) apparatus (figure taken from Klenner et al. (2019)).

(Kempf et al., 2014). The principle of delayed extraction allows the correlation of combinations of delay times and laser energy densities of different impact velocities of ice grains onto spaceborne detectors (Klenner et al., 2019).

The LILBID setup is calibrated daily using a solution of 10^{-6} M NaCl at three different delay times and laser intensities in order to quantify any potential contaminants in the system and to ensure reproducibility of the spectra. In general, mass spectra of organic compounds analyzed in LILBID can exhibit features from various cationic fragments as well as contamination from trace amounts (sub-ppm) of Na and K. This effect is generally well-quantified in earlier work (Khawaja et al., 2019; Klenner et al., 2019).

The signal produced by the ions on the detector is amplified, digitized, and recorded on a computer, which plots m/z values against relative ion yields to produce a mass spectrum. The signal-to-noise ratio is improved by averaging 500 single spectra to produce each coadded spectrum. A number of previous works have demonstrated that coadded LILBID spectra of one compositional type are applicable to in situ mass spectra from CDA (e.g., Klenner et al., 2019; Klenner, Postberg, Hillier, Khawaja, Cable, et al., 2020; Klenner, Postberg, Hillier, Khawaja, Reviol, et al., 2020). The threshold for peak retention in the mass spectra was set at 0.005%. Recorded mass spectra are archived in a comprehensive spectral LILBID database and aid planning for future space missions to icy moons (Klenner et al., 2022).

3. Data Sets and Selection Criteria

In this work, benzoic acid, and two of its isomeric derivatives, 2,3-DHBA and 2,5-DHBA, have been investigated with LILBID-TOF mass spectrometry. Each compound was injected into LILBID as an aqueous solution of concentration 0.025 M, significantly below the solubility limits of these species, at a flow rate of 0.23 mL min^{-1}. Three different simulated impact velocity regimes were studied in this work—henceforth called low, intermediate, and high—because different impact speeds of ice grains can produce fundamentally different spectral appearances even when the grains have the same composition (Klenner et al., 2019). The low velocity simulation corresponds to an impact velocity ~4–6 km/s and is achieved by operating the laser at 92.0% intensity with a mass spectrometer delay time of 69 μs. The intermediate velocity ~6.5–8.5 km/s is simulated with 96.2% laser intensity

and 55-μs delay time, while the high velocity regime corresponds to ~9–11 km/s and is simulated with 100% laser intensity and 43-μs delay time. Ions were measured in both the positive and negative modes; the importance of using both modes in analyzing organic-containing ice grains and searching for biosignatures was demonstrated in Klenner, Postberg, Hillier, Khawaja, Cable, et al. (2020) and Dannenmann et al. (2022). Similarly, the SUDA instrument aboard Europa Clipper will also measure ions in both polarities.

4. Results

Given that three different impact speeds were simulated for the three compounds and analyzed in two different ion modes (positive and negative), the mass spectra have been grouped by velocity for the sake of comparison. Figures 3–5 detail the positive mode spectra for the simulated low, intermediate, and high velocities, respectively, while Figures 6–8 detail the corresponding negative ion mode spectra. In all spectra, pure water cluster peaks are labeled in blue, organic/water cluster peaks are labeled in black, and pure organic ions and fragments are labeled in red. Tables 1–3 detail the m/z values of the peaks in the corresponding positive mode spectra, while Tables 4–6 detail the corresponding negative mode peaks. Note that only the peaks corresponding to organic species are listed in the tables.

4.1. Positive Ion Mode

In positive spectra, pure water cluster peaks at higher impact velocities appear at m/z values 19, 37, with intermediate velocities extending up to m/z 55 and 73, and lower velocities including peaks at m/z 91, 109, and potentially 127. Water clustering $[(H_3O)^+H_2O_{1,2,3...}]$ in the positive ion mode of LILIBD-TOF-MS has been discussed extensively in Khawaja et al. (2019) and Klenner et al. (2019), and our observations that water clustering is suppressed at higher impact velocities is in agreement with earlier results. Similarly, many organic-water clusters form in LILBID, usually distinguishable by spacings of 18 u, equivalent to the molecular mass of water, between peaks in the spectrum. Organic-water clusters follow a general trend of decreasing in number and intensity with increasing velocity.

The low velocity positive mode spectra for benzoic acid, 2,3-DHBA, and 2,5-DHBA are detailed in Figure 3. In the benzoic acid spectrum, the protonated ion peak at m/z 123 represents the species $[M+H]^+$ and the peak at m/z 105 is the fragment following the loss of a water molecule $[M+H−H_2O]^+$. The 2,3-DHBA and 2,5-DHBA spectra exhibit significant numbers of peaks at identical m/z values, but at varying abundances. A peaks at m/z 273 correspond to the dimer fragment $[2M+H−2H_2O]^+$, while the peak at m/z 155 represents the protonated ion $[M+H]^+$. Fragment species at m/z 137, 109, and 81 are tentatively assigned to $[M+H−H_2O]^+$, $[M+H−H_2O−CO]^+$, and $[M+H−H_2O−2CO]^+$, respectively.

Intermediate velocity spectra, recorded in the positive mode, are detailed in Figure 4. The benzoic acid spectrum exhibits a protonated ion $[M+H]^+$ peak at m/z 123, and displays fragments at m/z 105, following the loss of water, and m/z 77, following the further loss of CO—i.e., $[M+H−H_2O]^+$ and $[M+H−H_2O−CO]^+$, respectively. The DHBA spectra at this velocity are almost identical to each other, with the only exception being the fragmented dimer species at m/z 273 in the 2,5-DHBA spectrum, which has the same composition as above. Further mass lines at m/z 155, 137, 109, and 81 are assigned to the same species as above. In addition to these peaks, there are also signals at the lower masses of m/z 63 and 53, which are assigned to $[C_5H_3]^+$ and $[C_4H_5]^+$, respectively.

The higher velocity positive mode spectra are detailed in Figure 5 and exhibit far fewer organic-water clusters than lower velocities. There are pure organic fragments for benzoic acid once again at m/z 105 and 77, with additional peaks at m/z 51 from $[C_4H_3]^+$ and m/z 2 from $[H_2]^+$. The two DHBA spectra here exhibit identical features, with peaks at m/z 137, 109, 81, and 53 assigned to the same species as above. There is an additional feature at m/z 65, which likely originates from $[C_5H_5]^+$.

4.2. Negative Ion Mode

The negative mode spectra are detailed in Figures 6–8 and exhibit significant differences from their positive counterparts. The patterns of water clustering observed here are similar in nature to the positive spectra, but differ by masses of 2 u, owing to the deprotonation process involved in anion formation, as opposed to protonation in cation generation. Higher velocity spectra include water cluster peaks at m/z 17 and 35, with intermediate velocities including additional peaks at m/z 53, 71, and 89, while low velocities extend up to m/z 107 and 125.

There appear to be far more peaks related to dimer species for both benzoic acid and the DHBAs in the anionic low velocity regime, shown in Figure 6. In the benzoic acid spectrum, the peak at m/z 243 represents the dimer species $[2M−H]^-$, the peak at m/z 121 relates to the deprotonated molecule $[M−H]^-$, and the lower mass peak

Figure 3. Low velocity cationic mass spectra for (a) benzoic acid, (b) 2,3-DHBA, and (c) 2,5-DHBA. Pure water cluster peaks are labeled in blue, organic/water cluster peaks are labeled in black, and pure organic ions and fragments are labeled in red.

at m/z 77 is assigned to $[C_6H_5]^-$. The two DHBA compounds exhibit identical near-peaks with far more fragmentation than observed in the positive mode. Peaks at m/z 307, 289, and 245 all relate to the dimer fragments $[2M-H]^-$, $[2M-H-H_2O]^-$, and tentatively $[2M-H-H_2O-CO_2]^-$, respectively. The peak at m/z 153 is assigned to the deprotonated molecule $[M-H]^-$. Further fragments species at m/z 135 and 109 are assigned to $[M-H-H_2O]^-$ and $[M-H-CO_2]^-$, respectively.

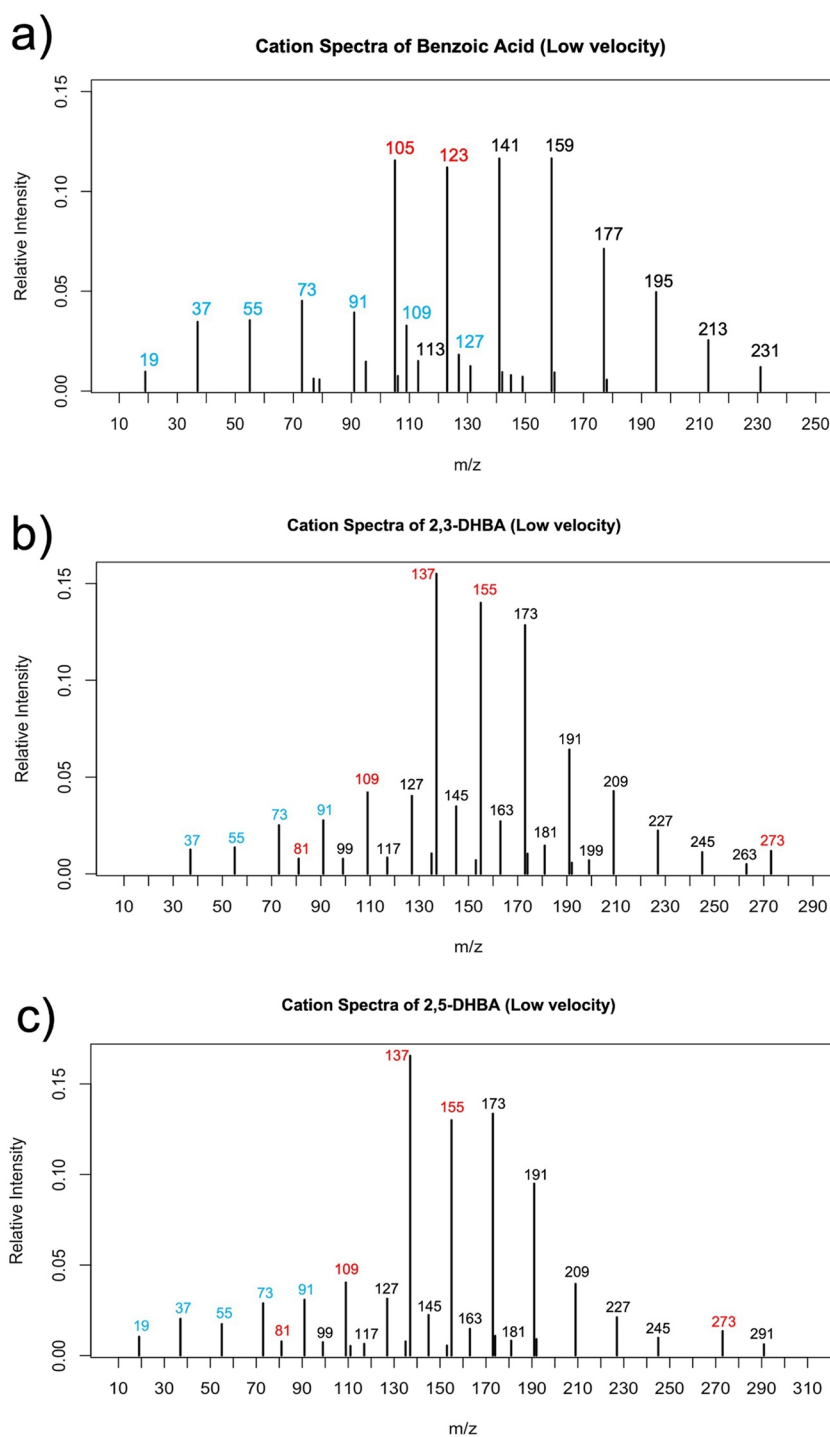**Figure 4.** Intermediate velocity cationic spectra for (a) benzoic acid, (b) 2,3-DHBA, and (c) 2,5-DHBA. Pure water cluster peaks are labeled in blue, organic/water cluster peaks are labeled in black, and pure organic ions and fragments are labeled in red.

The intermediate velocity spectra, from the negative ion mode, are detailed in Figure 4. The benzoic acid spectrum exhibits just two peaks, at *m/z* 121 and 77, assigned to the same species as above. The DHBA spectra now appear to exhibit significant differences at this velocity. Common, previously observed, peaks appear at *m/z* 153, 109, and 81. The 2,3-DHBA spectrum, however, also exhibits peaks at *m/z* 245 and 65, whereas the 2,5-DHBA spectrum

Figure 5. High velocity cationic spectra for (a) benzoic acid, (b) 2,3-DHBA, and (c) 2,5-DHBA. Pure water cluster peaks are labeled in blue, organic/water cluster peaks are labeled in black, and pure organic ions and fragments are labeled in red.

does not. These peaks are assigned to $[2M-H-H_2O-CO_2]^-$ and $[M-H-2CO_2]^-$, respectively. Similarly, the 2,5-DHBA spectrum also exhibits additional peaks, not observed with 2,3-DHBA, at m/z values 135 and 97. The former peak likely relates to $[M-H-H_2O]^-$ while the composition of the species at m/z 97 is unidentifiable.

Finally, the high velocity spectra recorded in the negative ion mode exhibit significantly different spectral features than previously observed. The only organic peak observed in the benzoic acid spectrum is an unidentified species

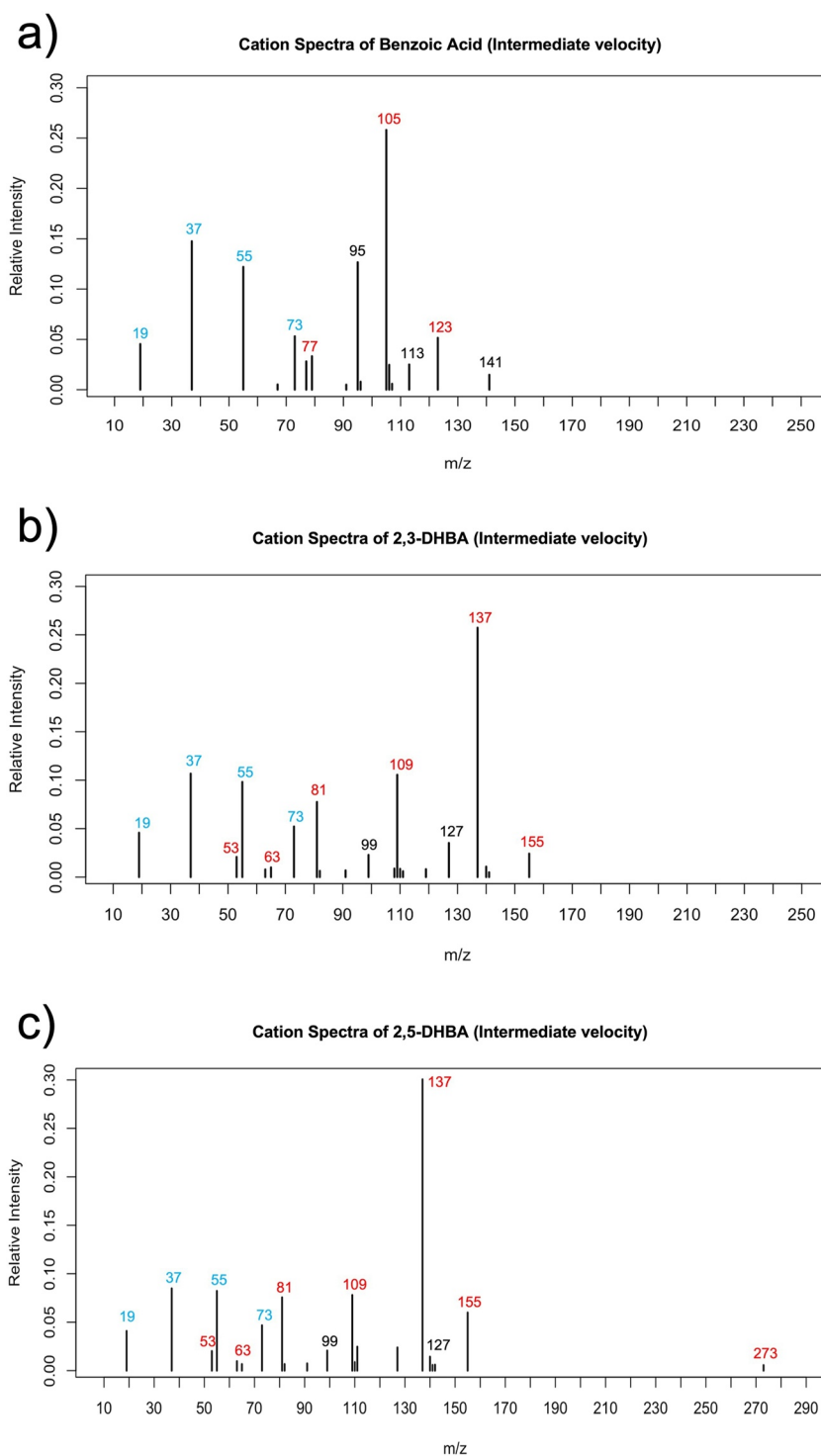**Figure 6.** Low velocity anionic spectra for (a) benzoic acid, (b) 2,3-DHBA, and (c) 2,5-DHBA. Pure water cluster peaks are labeled in blue, organic/water cluster peaks are labeled in black, and pure organic ions and fragments are labeled in red.

at m/z 11. The only peak in the 2,3-DHBA spectrum relates to the fragment $[M-H-H_2O-CO]^-$ at m/z 107. This is also observed in the 2,5-DHBA spectrum alongside additional peaks at m/z 79, 51, 41. These peaks are assigned to the species $[M-H-H_2O-2CO]^-$, $[M-H-H_2O-3CO]^-$, $[C_3H_5]^-$. A further peak at m/z 25 is tentatively assigned to deprotonated acetylene $[C_2H]^-$, while the composition of the species at m/z 10 is unidentifiable and may be an experimental artifact.

Figure 7. Intermediate velocity anionic spectra for (a) benzoic acid, (b) 2,3-DHBA, and (c) 2,5-DHBA. Pure water cluster peaks are labeled in blue, organic/water cluster peaks are labeled in black, and pure organic ions and fragments are labeled in red.
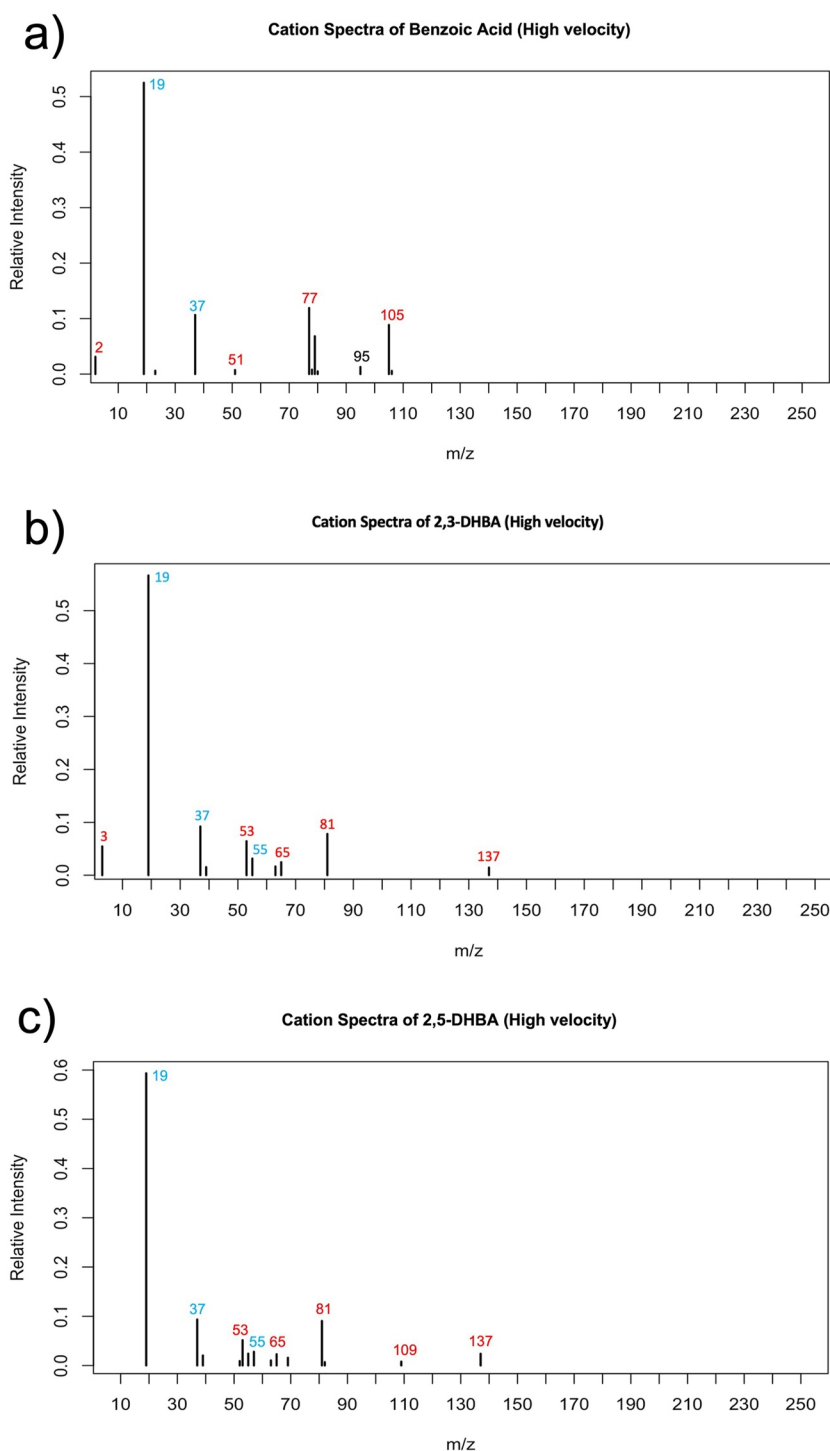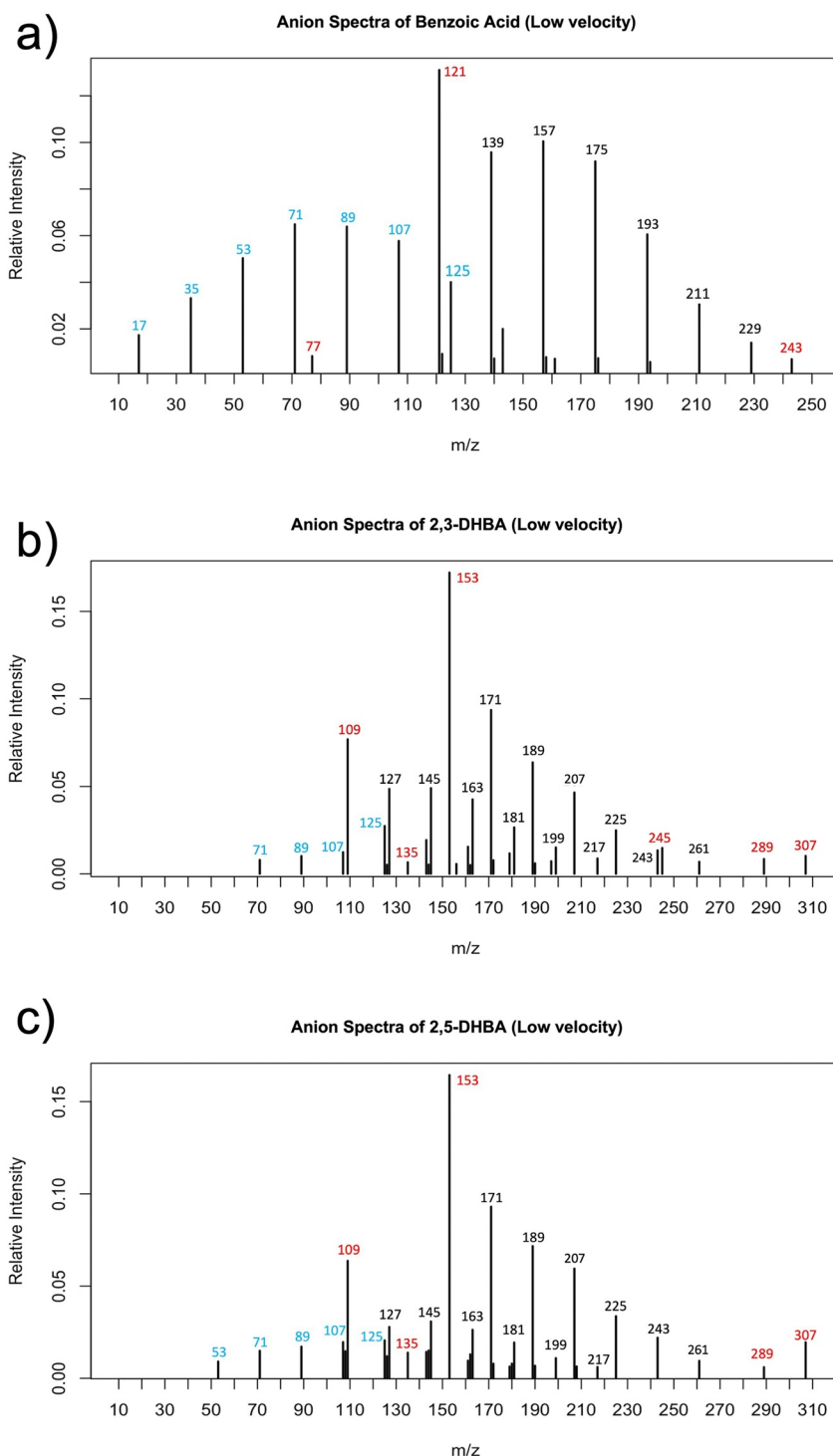
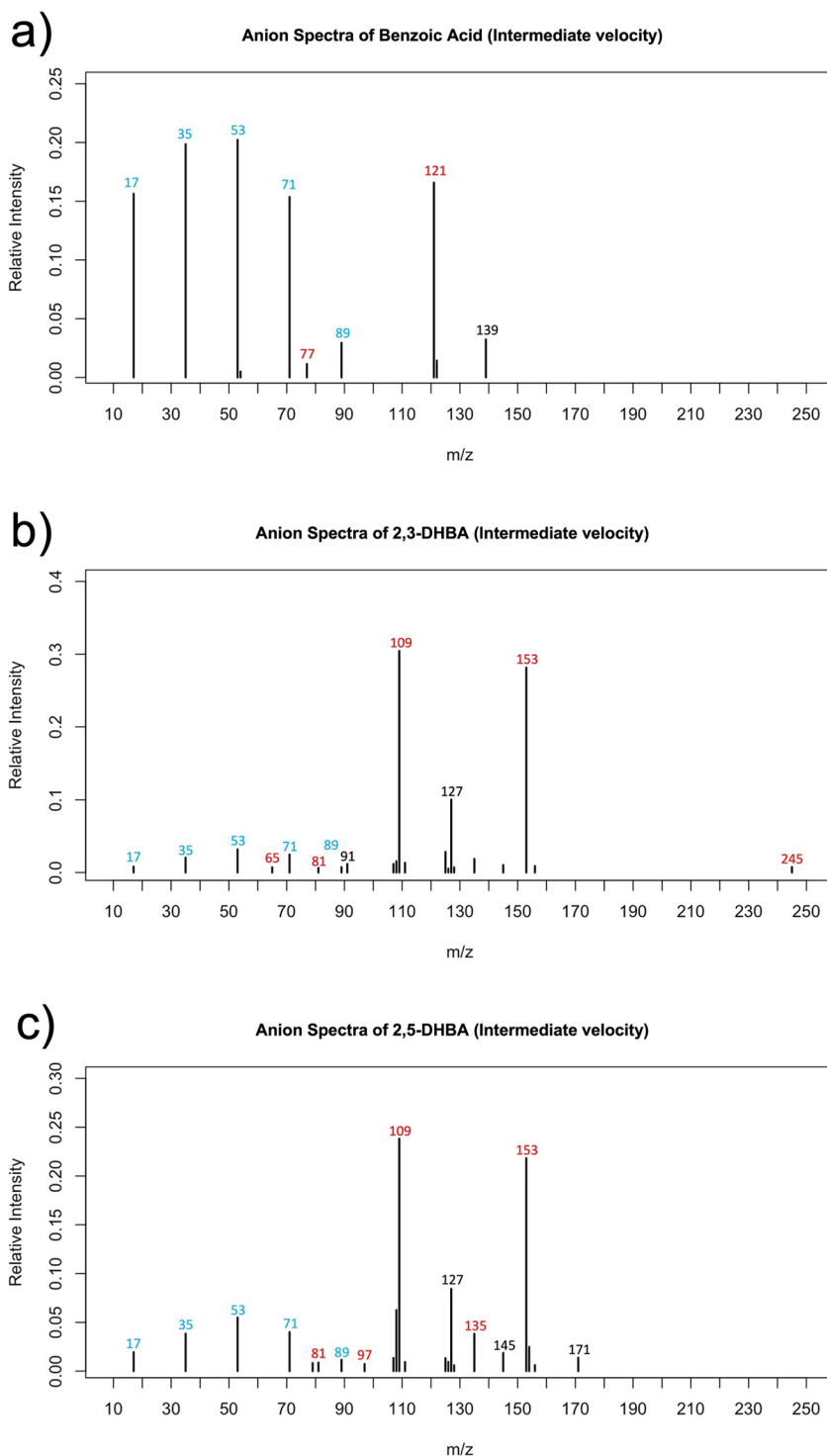**Figure 8.** High velocity anionic spectra for (a) benzoic acid, (b) 2,3-DHBA, and (c) 2,5-DHBA. Pure water cluster peaks are labeled in blue, organic/water cluster peaks are labeled in black, and pure organic ions and fragments are labeled in red.
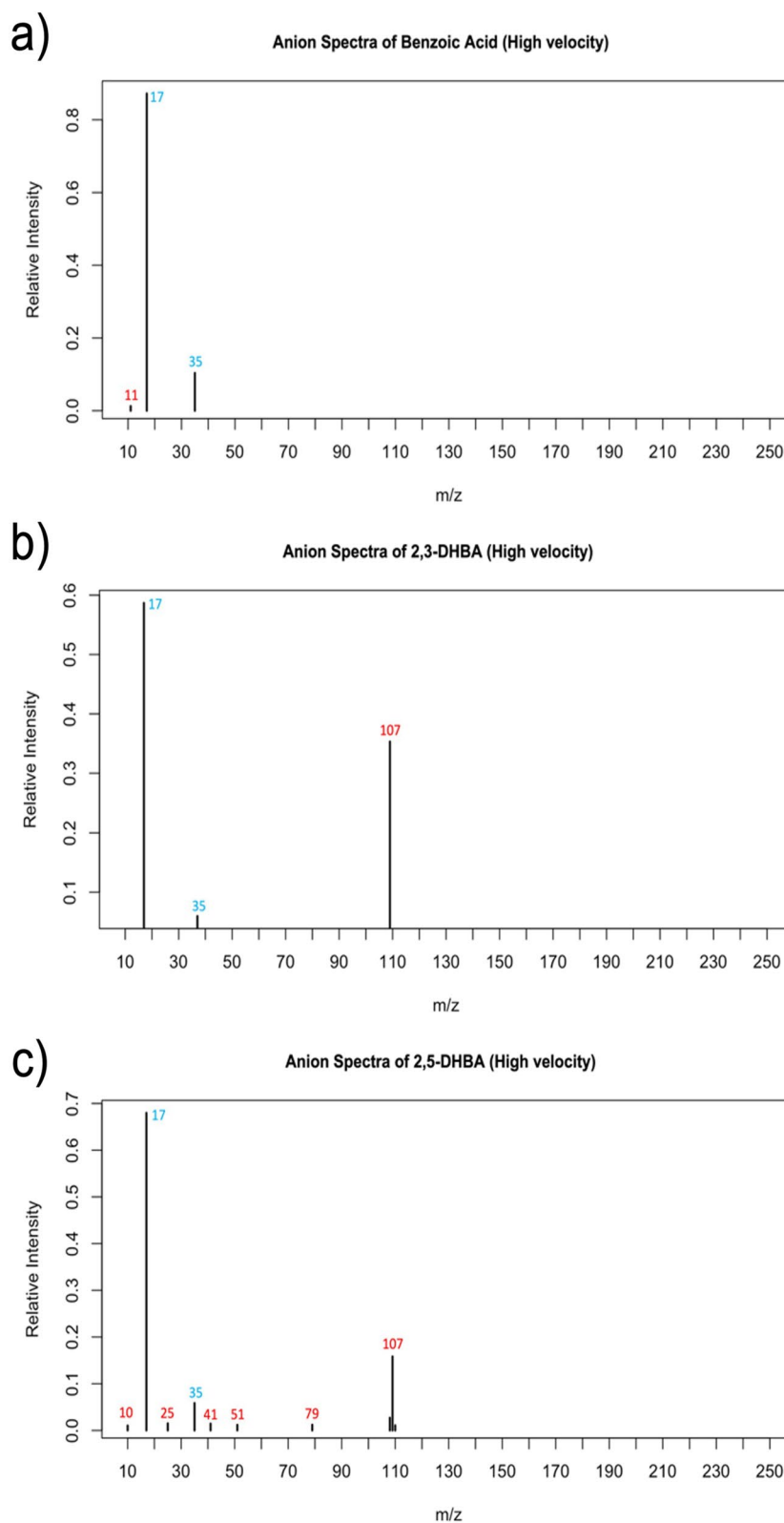
Table 1
Organic-Related Features in the Low Velocity Cationic Mass Spectra

	Benzoic acid		2,3-DHBA		2,5-DHBA	
m/z	Fragment	Relative intensity	Fragment	Relative intensity	Fragment	Relative intensity
273	–	–	$[2M+H-2H_2O]^+$	0.0119	$[2M+H-2H_2O]^+$	0.0135
155	–	–	$[M+H]^+$	0.1400	$[M+H]^+$	0.1300
137	–	–	$[M+H-H_2O]^+$	0.1551	$[M+H-H_2O]^+$	0.1656
123	$[M+H]^+$	0.1120	–	–	–	–
109	–	–	$[M+H-H_2O-CO]^+$	0.0430	$[M+H-H_2O-CO]^+$	0.0406
105	$[M+H-H_2O]^+$	0.1155	–	–	–	–
81	–	–	$[M+H-H_2O-2CO]^+$	0.0079	$[M+H-H_2O-2CO]^+$	0.0078

Note. A "–" entry corresponds to an absent peak in the spectrum. "M" denotes the molecular ion.

5. Discussion

5.1. Mass Spectral Analysis

Significant differences are observed between the benzoic acid and DHBA spectra across all velocities in both positive and negative modes. There are no common organic-related features between benzoic acid and either DHBA spectra at any velocity across both modes. The additional hydroxyl groups present on the DHBA rings thus seem to have a greater influence on fragmentation than aromatic cleavage does, although this does occur in some spectra. While it is clear that the DHBA spectra must arise from very similar compounds, it is not straightforward to decipher the relationship between benzoic acid and the DHBAs from the mass spectra alone.

There also appears to be a correlation between the simulated impact velocity and the degree and diversity of differences between the 2,3-DHBA and 2,5-DHBA spectra produced. There is virtually no difference between the fragmentation pattern exhibited by both DHBAs during low velocity impacts. Intermediate velocities yield spectra that exhibit greater differences, particularly in the negative mode. Higher impact velocities appear to only exhibit significant spectral differences in the negative mode. Therefore, collecting data over a range of impact velocities will be advantageous for the elucidation of structural features from impact ionization mass spectrometers. The estimations of impact speed ranges for CDA based on the experimental parameters of LILBID are well-defined (Klenner et al., 2019), but SUDA will be able to determine such velocities far more precisely than CDA. This more precise determination will further improve confidence in mass spectral analysis for spaceborne instruments.

Table 2
Organic-Related Features in the Intermediate Velocity Cationic Mass Spectra

	Benzoic acid		2,3-DHBA		2,5-DHBA	
m/z	Fragment	Relative intensity	Fragment	Relative intensity	Fragment	Relative intensity
273	–	–	–	–	$[2M+H-2H_2O]^+$	0.0056
155	–	–	$[M+H]^+$	0.0243	$[M+H]^+$	0.0600
137	–	–	$[M+H-H_2O]^+$	0.2574	$[M+H-H_2O]^+$	0.3006
123	$[M+H]^+$	0.0517	–	–	–	–
109	–	–	$[M+H-H_2O-CO]^+$	0.1056	$[M+H-H_2O-CO]^+$	0.0781
105	$[M+H-H_2O]^+$	0.2582	–	–	–	–
81	–	–	$[M+H-H_2O-2CO]^+$	0.0776	$[M+H-H_2O-2CO]^+$	0.0756
77	$[M+H-H_2O-CO]^+$	0.0282	–	–	–	–
63	–	–	$[C_5H_3]^+$	0.0079	$[C_5H_3]^+$	0.0098
53	–	–	$[C_4H_5]^+$	0.0208	$[C_4H_5]^+$	0.0409

Note. A "–" entry corresponds to an absent peak in the spectrum. "M" denotes the molecular ion.

Table 3
Organic-Related Features in the High Velocity Cationic Mass Spectra

	Benzoic acid		2,3-DHBA		2,5-DHBA	
m/z	Fragment	Relative intensity	Fragment	Relative intensity	Fragment	Relative intensity
137	–	–	$[M+H-H_2O]^+$	0.0145	$[M+H-H_2O]^+$	0.0240
109	–	–	–	–	$[M+H-H_2O-CO]^+$	0.0080
105	$[M+H-H_2O]^+$	0.0888	–	–	–	–
81	–	–	$[M+H-H_2O-2CO]^+$	0.0782	$[M+H-H_2O-2CO]^+$	0.0906
77	$[M+H-H_2O-CO]^+$	0.1192	–	–	–	–
65	–	–	$[C_5H_5]^+$	0.0247	$[C_5H_5]^+$	0.0231
53	–	–	$[C_4H_5]^+$	0.0644	$[C_4H_5]^+$	0.0515
51	$[C_4H_3]^+$	0.0075	–	–	–	–
2	$[H_2]^+$	0.0313	–	–	–	–

Note. A "–" entry corresponds to an absent peak in the spectrum. "M" denotes the molecular ion.

There is a degree of uncertainty surrounding the peak at m/z 109, currently assigned to the ion $[M+H-H_2O-CO]^+$, that appears in some positive spectra for the DHBAs. This species lies 45 u below the nonprotonated molecular ion (at m/z 154) which may imply the process of decarboxylation or successive losses of OH and then CO, in which case the species would appear as $[M-COOH]^+$. However, LILBID favors the production of protonated ions (Khawaja et al., 2022; Klenner et al., 2019), which precedes the loss of water and successive CO molecules in this instance. Losses of 28 u from DHBA in matrix-based mass spectrometry due to the liberation of CO molecules are well-established in the literature (Hsu et al., 2014), suggesting that multiple fragmentation pathways may take place with varying likelihoods of occurrence. Other potentially interfering fragments and clusters are listed in Tables S1–S3 in Supporting Information S1. It is important to note that patterns of clustering between water and organics are an identifying feature that can assist in tracking various structural features across a mass spectrum and elucidating compositions.

5.2. Role of Hydrogen Bonding

In the positive ion mode, the 2,3-DHBA and 2,5-DHBA spectra are almost identical, but there is one key difference. The lack of intramolecular hydrogen bonding in 2,5-DHBA particularly influences the spectra at low and intermediate velocities, with a peak at m/z 273 i.e., absent in the 2,3-DHBA spectrum. This peak is assigned to the

Table 4
Organic-Related Features in the Low Velocity Anionic Spectra

	Benzoic acid		2,3-DHBA		2,5-DHBA	
m/z	Fragment	Relative intensity	Fragment	Relative intensity	Fragment	Relative intensity
307	–	–	$[2M-H]^-$	0.0103	$[2M-H]^-$	0.0196
289	–	–	$[2M-H-H_2O]^-$	0.0086	$[2M-H-H_2O]^-$	0.0061
245	–	–	$[2M-H-H_2O-CO_2]^-$	0.0149	–	–
243	$[2M-H]^-$	0.0071	–	–	–	–
153	–	–	$[M-H]^-$	0.1723	$[M-H]^-$	0.1644
135	–	–	$[M-H-H_2O]^-$	0.0067	$[M-H-H_2O]^-$	0.0139
121	$[M-H]^-$	0.1311	–	–	–	–
109	–	–	$[M-H-CO_2]^-$	0.0769	$[M-H-CO_2]^-$	0.0637
77	$[C_6H_5]^-$	0.0084	–	–	–	–

Note. A "–" entry corresponds to an absent peak in the spectrum. "M" denotes the molecular ion.

Table 5
Organic-Related Features in the Intermediate Velocity Anionic Mass Spectra

m/z	Benzoic acid		2,3-DHBA		2,5-DHBA	
	Fragment	Relative intensity	Fragment	Relative intensity	Fragment	Relative intensity
245	–	–	$[2M-H-H_2O-CO_2]^-$	0.0076	–	–
153	–	–	$[M-H]^-$	0.2815	$[M-H]^-$	0.2183
135	–	–	–	–	$[M-H-H_2O]^-$	0.0383
121	$[M-H]^-$	0.1658	–	–	–	–
109	–	–	$[M-H-CO_2]^-$	0.3045	$[M-H-CO_2]^-$	0.2383
97	–	–	–	–	Unidentifiable	0.0074
81	–	–	$[M-H-CO_2-CO]^-$	0.0064	$[M-H-CO_2-CO]^-$	0.0087
77	$[C_6H_5]^-$	0.0115	–	–	–	–
65	–	–	$[M-H-2CO_2]^-$	0.0073	–	–

Note. A "–" entry corresponds to an absent peak in the spectrum. "M" denotes the molecular ion.

dimer species $[2M+H-2H_2O]^+$ through consideration of intermolecular and intramolecular bonding. 2,3-DHBA has a greater number of intramolecular bonds, shown in Figure 9, most notably the additional hydrogen bond that can occur due to the proximity of the two hydroxyl groups on C_2 and C_3. This additional hydrogen bond is absent in 2,5-DHBA as the hydroxyl groups are too far apart, rendering any interactions between them negligible, although the presence of this bond will influence water clustering. In 2,5-DHBA, there is thus an additional hydrogen bond available for intermolecular interactions. Consequently, 2,5-DHBA may exhibit an affinity for dimer formation via hydrogen bonding with other molecules during impact ionization, as previously reported by Okabe and Kyoyama (2001). The low amplitude of this peak may be explained by the necessity of two 2,5-DHBA molecules being in the correct orientation for dimer formation at any given instant. This likely has a low probability of occurrence during impact ionization, hence the low abundance of this fragment. A similar effect is observed in the low and intermediate velocity negative modes, where the same peaks are present in both 2,3-DHBA and 2,5-DHBA spectra but at lower amplitudes in the latter. At low velocities, the DHBA spectra are almost identical in the cationic mode—the only differences lie in the acid-water clustering patterns. This is also likely due to the difference in intermolecular hydrogen bonding interactions between the solute DHBAs and the solvent water molecules.

The patterns of pure water clustering exhibit the same velocity dependence across all species and ion modes. In positive ion mode, amplitudes of water clusters peaks in benzoic acid spectrum are relatively higher than in 2,3-DHBA and 2,5-DHBA spectra at lower and intermediate velocities. However, this difference in the amplitudes of water clusters is significantly pronounced in negative ion mode spectra. This shows that negative ion mode is

Table 6
Organic-Related Features in the High Velocity Anionic Mass Spectra

m/z	Benzoic acid		2,3-DHBA		2,5-DHBA	
	Fragment	Relative intensity	Fragment	Relative intensity	Fragment	Relative intensity
109	–	–	$[M-H-H_2O-CO]^-$	0.3533	$[M-H-H_2O-CO]^-$	0.1584
79	–	–	–	–	$[M-H-H_2O-2CO]^-$	0.0124
51	–	–	–	–	$[M-H-H_2O-3CO]^-$	0.0121
41	–	–	–	–	$[C_3H_5]^-$	0.0147
25	–	–	–	–	$[C_2H]^-$	0.0152
11	Unidentifiable	0.0128	–	–	–	–
10	–	–	–	–	Unidentifiable	0.0105

Note. A "–" entry corresponds to an absent peak in the spectrum. "M" denotes the molecular ion.
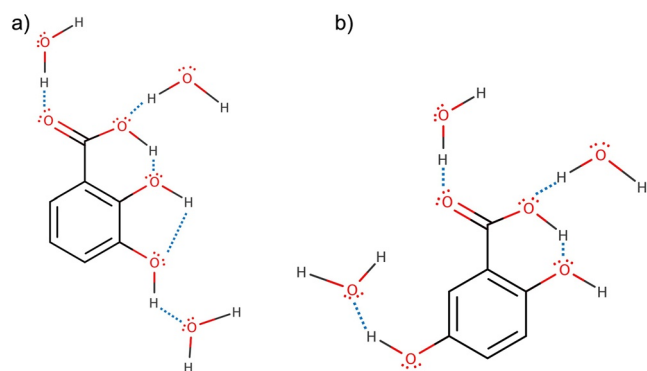
Figure 9. The possible acid-water and intramolecular hydrogen bonding regimes that may occur in solute (a) 2,3-DHBA, and (b) 2,5-DHBA. The blue dotted lines represent hydrogen bonds. Note the intramolecular hydrogen bond in 2,3-DHBA between the hydroxyl groups is absent in 2,5-DHBA.

more favorable for pure water clustering for benzoic acids as compared to its derivative compounds. The organic-water clusters, however, exhibit significant differences between benzoic acid and the DHBA spectra. One possible explanation for this is that the presence of the polar OH group at position 2 on the benzene ring disrupts the hydrogen bonding that would normally occur with the carboxyl group. The intramolecular bonding exhibited by 2,3-DHBA may prevent an additional water molecule from binding with the carboxyl group as is the case in 2,5-DHBA. Indeed, it may be the case that intramolecular interactions within molecules influence fragmentation patterns and the types of cleavage which can occur. Figure 9 details the lack of intramolecular bonding around the OH group at position 5 in 2,5-DHBA and the distance between the 2-OH and 3-OH groups in 2,3-DHBA may mean that the hydrogen bonding there is too weak to influence fragmentation. Yamagaki et al. (2016) investigated the mechanisms for anion generation of DHBA isomers in matrix-assisted laser desorption/ionization (MALDI) and found that a singular proton was trapped between the carboxyl and *ortho*-hydroxyl group in 2,3-DHBA and 2,5-DHBA. This suggests that hydrogen bonding is much stronger between the carboxyl and 2-OH group than it is between hydroxyl groups. Future work should look to investigate the fragmentation patterns of other DHBA isomers such as 3,4-DHBA and 3,5-DHBA along with other 2,X-DHBAs to characterize the influence of OH proximity to the –COOH group.

5.3. Implications for Icy Moons

Aqueous benzoic acid often occurs in the form of a salt dissolved in water, most commonly an alkali metal benzoate. The presence of sodium and potassium within ice grains originating from Enceladus has been considered evidence for dissolved salts in the ocean (Postberg et al., 2009). As a result, if benzoic acid is present on ocean worlds, its dominant form may be sodium benzoate. While benzoic acid is generally poorly soluble in water, the salt form dissolves more readily. At higher temperatures (~330 K), however, benzoic acid becomes more soluble (Muhammad et al., 2020)—meaning that higher temperature regions of the ocean, such as hydrothermal systems, may facilitate the dissolution of benzoic acid. Through salt-acid interactions on its journey through the ocean toward cooler temperatures nearing the surface, conversion to sodium benzoate may take place through interactions with dissolved ionic substances (i.e., Burdock, 2010). It should be noted, however, that alkali metal salts have been known to modify/suppress organic signatures in mass spectra (Piwowar et al., 2009). Thus, if benzoic acid is present on Enceladus, its features may be modified in the presence of alkali metal salts also dissolved in the ocean. Recent work from Schulze et al. (2022) suggests that solubility and salinity play key roles in the fragmentation pathways of amino acids in ice grains, which may be extendable to other classes of organics. Future work should repeat these experiments with salt-rich matrices, representing both type III ice grains from Enceladus and particles sputtered from the salty surface of Europa.

This work continues to develop the understanding of impact ionization mass spectrometers in future space missions to icy moons. Other substituent groups should be investigated to verify if intramolecular hydrogen bonding is indeed an important factor in fragmentation patterns. Amino acids are of particular interest, especially given the complementary role of chiral asymmetry and structural isomerism (alongside isotopic ratios; Glavin et al., 2020) as a biosignature and their vital role in biochemistry. For isobaric compounds, those with the same mass but different molecular structures, it may be challenging to distinguish one from the other from the molecular ion peak alone, provided it is even retained in the impact ionization process. Fragmentation patterns must be considered in order to infer the molecular structure. SUDA will be capable of detecting amino acids, for instance, but many amino acids have similar masses, and some are structural isomers of each other (i.e., leucine/isoleucine, 131 u). Therefore, analytical techniques and instrument calibration methods for the discrimination of isobaric and even isomeric compounds are important for future astrobiology investigations. Further work into the discrimination of isobaric compounds with LILBID is also recommended as a complementary study—the identification of fragmentation pathways may be beneficial in elucidating the composition of species in ice grains, particularly to those missions encountering a wider range of impact velocities. Furthermore, a mass analyzer with a higher mass

resolution, such as an Orbitrap-based instrument (e.g., Sanderink et al., 2023), would help differentiate between molecules that appear at the same integer mass in our experiments.

6. Conclusions

We investigated the LILBID mass spectra of benzoic acid and two of its derivatives, 2,3-dihydroxybenzoic acid and 2,5-dihydroxybenzoic acid to discriminate the composition of single ring aromatic compounds from their isomeric derivatives, in an effort to simulate their impact ionization mass spectra from a spaceborne instrument. Three different impact velocities of ice grains in space were simulated by varying the laser and delay time settings of LILBID, coupled with a mass spectrometer operating in both the positive and negative ion modes.

We conclude that, at all velocities, the DHBA spectra are significantly different from that of benzoic acid, with no common features between them. It is thus simple to distinguish between the parent and derivative compounds. It is challenging to decipher the relationship between the parent benzoic acid and its derivatives from LILBID mass spectra alone due to the lack of common spectral features between them, but additional analytical techniques may give insights in this regard—i.e., Khawaja et al. (2022), where differences in spectral features can be used in a complementary way to relate their composition. Between the 2,3-DHBA and 2,5-DHBA spectra, there are fewer differences at all velocities in the positive mode and at low velocities in the negative mode. The exceptional presence of a dimer species in the intermediate velocity positive 2,5-DHBA spectrum is explained by consideration of the intramolecular hydrogen bonding regimes in each compound. We conclude that differences in the position of the second hydroxyl group in 2,3-dihydroxybenzoic acid and 2,5-dihydroxybenzoic acid only influence fragmentation in negative spectra at intermediate and high velocities. There is some affinity for dimer formation in positive low velocity spectra, although only at low intensities, suggesting that this process is less likely to occur and may be due to the nature of the solution used in LILBID.

Distinguishing between the parent benzoic acid compound and its disubstituted derivatives is generally straightforward given the significant differences between the spectra. In general, it is possible to distinguish between structural isomers if the possible molecular structures are known. By considering hydrogen bonding regimes, the affinity for formation of dimer and more complex oligomer species, and the subsequent influence on the spectrum, we find that a logical deduction of the isomers is possible. However, for species of unknown composition, it is difficult to assign spectra to any given isomer. Intermediate impact velocities are low enough to retain similarities in lower mass fragmentation between the different isomers but remain significant enough to exhibit the key difference in dimer formation. Differences in the spectra between 2,3-DHBA and 2,5-DHBA are generally enhanced in the anionic mode. For spaceborne impact ionization mass spectra, the identity of the general species must first be ascertained from rule-based fragmentation pattern analysis and comparison to reference spectra, after which structural properties of the isomers can be inferred.

Future work should consider methods to further distinguish between isomeric and isobaric compounds—the expansion of this work to the isomeric derivatives of other molecular classes such as amino acids or indeed other DHBA isomers is required to further clarify characteristics and rules of mass spectral analysis for future missions to icy moons. In addition, the different types of ice grains that originate from Enceladus vary in salt and organic content, so the influence of different concentrations and salinities should also be investigated in the future. Similarly, grains ejected from the surface of Europa are likely to be salt-rich, so matrix or suppression effects may influence the spectral appearance. Additional work using the LILBID setup at FUB will address this area.

Data Availability Statement

All mass spectral data reported in this work are available at http://dx.doi.org/10.17169/refubium-37960. They are also available and maintained in the online LILBID database https://lilbid-db.planet.fu-berlin.de/ outlined in Klenner et al. (2022).

References

Barge, L. M., Flores, E., Baum, M. M., VanderVelde, D. G., & Russell, M. J. (2019). Redox and pH gradients drive amino acid synthesis in iron oxyhydroxide mineral systems. *Proceedings of the National Academy of Sciences of the United States of America*, *116*(11), 4828–4833. https://doi.org/10.1073/pnas.1812098116

Burdock, G. A. (2010). *Fenaroli's handbook of flavor ingredients* (6th ed.). CRC Press.

Charvat, A., & Abel, B. (2007). How to make big molecules fly out of liquid water: Applications, features and physics of laser assisted liquid phase dispersion mass spectrometry. *Physical Chemistry Chemical Physics*, *9*(26), 3335. https://doi.org/10.1039/b615114k

Cobb, D. T. (Ed.) (2014). *Polyphenols: Food sources, bioactive properties, and antioxidant effects*. Nova Science Publishers, Inc.

Cody, G. D., Boctor, N. Z., Filley, T. R., Hazen, R. M., Scott, J. H., Sharma, A., & Yoder, H. S. (2000). Primordial carbonylated iron-sulfur compounds and the synthesis of pyruvate. *Science*, *289*(5483), 1337–1340. https://doi.org/10.1126/science.289.5483.1337

Dannenmann, M., Klenner, F., Bönigk, J., Pavlista, M., Napoleoni, M., Hillier, J., et al. (2022). Toward detecting biosignatures of DNA, lipids, and metabolic intermediates from bacteria in ice grains emitted by Enceladus and Europa. *Astrobiology*, *23*(1), 63–75. https://doi.org/10.1089/ast.2022.0063

Glavin, D. P., Burton, A. S., Elsila, J. E., Aponte, J. C., & Dworkin, J. P. (2020). The search for chiral asymmetry as a potential biosignature in our solar system. *Chemical Reviews*, *120*(11), 4660–4689. https://doi.org/10.1021/acs.chemrev.9b00474

Grootveld, M., & Halliwell, B. (1988). 2,3-Dihydroxybenzoic acid is a product of human aspirin metabolism. *Biochemical Pharmacology*, *37*(2), 271–280. https://doi.org/10.1016/0006-2952(88)90729-0

Hand, K. P., Carlson, R. W., & Chyba, C. F. (2007). Energy, chemical disequilibrium, and geological constraints on Europa. *Astrobiology*, *7*(6), 1006–1022. https://doi.org/10.1089/ast.2007.0156

Hsu, H. C., Lu, I.-C., Lin, P.-H., Dyakov, Y. A., Bagchi, A., Lin, C.-Y., et al. (2014). Does decarboxylation make 2,5-dihydroxybenzoic acid special in matrix-assisted laser desorption/ionization? *Rapid Communications in Mass Spectrometry*, *28*(10), 1082–1088. https://doi.org/10.1002/rcm.6885

Hsu, H.-W., Postberg, F., Sekine, Y., Shibuya, T., Kempf, S., Horányi, M., et al. (2015). Ongoing hydrothermal activities within Enceladus. *Nature*, *519*(7542), 207–210. https://doi.org/10.1038/nature14262

Jia, X., Kivelson, M. G., Khurana, K. K., & Kurth, W. S. (2018). Evidence of a plume on Europa from Galileo magnetic and plasma wave signatures. *Nature Astronomy*, *2*(6), 459–464. https://doi.org/10.1038/s41550-018-0450-z

Juurlink, B. H., Azouz, H. J., Aldalati, A. M., Al Tinawi, B. M., & Ganguly, P. (2014). Hydroxybenzoic acid isomers and the cardiovascular system. *Nutrition Journal*, *13*(1), 63. https://doi.org/10.1186/1475-2891-13-63

Karas, M., Glückmann, M., & Schäfer, J. (2000). Ionization in matrix-assisted laser desorption/ionization: Singly charged molecular ions are the lucky survivors. *Journal of Mass Spectrometry*, *35*(1), 1–12. https://doi.org/10.1002/(SICI)1096-9888(200001)35:1<1::AID-JMS904>3.0.CO;2-0

Kempf, S., Altobelli, N., Briois, C., Grün, E., Horanyi, M., Postberg, F., et al. (2014). SUDA: A dust mass spectrometer for compositional surface mapping for a mission to Europa. *Paper presented at European Planetary Science Congress*. Cascais, Portugal.

Khawaja, N., Hillier, J., Klenner, F., Nölle, L., Zou, Z., Napoleoni, M., et al. (2022). Complementary mass spectral analysis of isomeric O-bearing organic compounds and fragmentation differences through analog techniques for spaceborne mass spectrometers. *The Planetary Science Journal*, *3*(11), 254. https://doi.org/10.3847/PSJ/ac97ed

Khawaja, N., Postberg, F., Hillier, J., Klenner, F., Kempf, S., Nölle, L., et al. (2019). Low-mass nitrogen-oxygen-bearing, and aromatic compounds in Enceladean ice grains. *Monthly Notices of the Royal Astronomical Society*, *489*(4), 5231–5243. https://doi.org/10.1093/mnras/stz2280

Kissel, J., Glasmachers, A., Grün, E., Henkel, H., Höfner, H., Haerendel, G., et al. (2003). Cometary and interstellar dust analyzer for comet Wild 2. *Journal of Geophysical Research*, *108*(E10), 8114. https://doi.org/10.1029/2003JE002091

Klenner, F., Postberg, F., Hillier, J., Khawaja, N., Cable, M. L., Abel, B., et al. (2020). Discriminating abiotic and biotic fingerprints of amino acids and fatty acids in ice grains relevant to ocean worlds. *Astrobiology*, *20*(10), 1168–1184. https://doi.org/10.1089/ast.2019.2188

Klenner, F., Postberg, F., Hillier, J., Khawaja, N., Reviol, R., Srama, R., et al. (2019). Analogue spectra for impact ionization mass spectra of water ice grains obtained at different impact speeds in space. *Rapid Communications in Mass Spectrometry*, *33*(22), 1751–1760. https://doi.org/10.1002/rcm.8518

Klenner, F., Postberg, F., Hillier, J., Khawaja, N., Reviol, R., Stolz, F., et al. (2020). Analog experiments for the identification of trace biosignatures in ice grains from extraterrestrial ocean worlds. *Astrobiology*, *20*(2), 179–189. https://doi.org/10.1089/ast.2019.2065

Klenner, F., Umair, M., Walter, S. H. G., Khawaja, N., Hillier, J., Nölle, L., et al. (2022). Developing a laser induced liquid beam ion desorption spectral database as reference for spaceborne mass spectrometers. *Earth and Space Science*, *9*, e02313. https://doi.org/10.1029/2022EA002313

Krüger, H., Strub, P., Srama, R., Kobayashi, M., Arai, T., Kimura, H., et al. (2019). Modelling DESTINY+ interplanetary and interstellar dust measurements en route to the active asteroid (3200) Phaethon. *Planetary and Space Science*, *172*, 22–42. https://doi.org/10.1016/j.pss.2019.04.005

Li, X., Svedin, E., Mo, H., Atwell, S., Dilkes, B. P., & Chapple, C. (2014). Exploiting natural variation of secondary metabolism identifies a gene controlling the glycosylation diversity of dihydroxybenzoic acids in *Arabidopsis thaliana*. *Genetics*, *198*(3), 1267–1276. https://doi.org/10.1534/genetics.114.168690

Martins, Z., Watson, J. S., Sephton, M. A., Botta, O., Ehrenfreund, P., & Gilmour, I. (2006). Free dicarboxylic and aromatic acids in the carbonaceous chondrites Murchison and Orgueil. *Meteoritics & Planetary Science*, *41*(7), 1073–1080. https://doi.org/10.1111/j.1945-5100.2006.tb00505.x

McMurtry, B. M., Saito, S. E. J., Turner, A. M., Chakravarty, H. K., & Kaiser, R. I. (2016). On the formation of benzoic acid and higher-order benzene carboxylic acids in interstellar model ice grains. *The Astrophysical Journal*, *831*(2), 174. https://doi.org/10.3847/0004-637X/831/2/174

Ménez, B., Pisapia, C., Andreani, M., Jamme, F., Vanbellingen, Q. P., Brunelle, A., et al. (2018). Abiotic synthesis of amino acids in the recesses of the oceanic lithosphere. *Nature*, *564*(7734), 59–63. https://doi.org/10.1038/s41586-018-0684-z

Muhammad, S., Sanam, S., Khan, H., Muhammad, A., & Sultana, S. (2020). Temperature dependent solubility of benzoic acid in aqueous phase and aqueous mixtures of aliphatic alcohols. *Zeitschrift für Physikalische Chemie*, *234*(11–12), 1771–1787. https://doi.org/10.1515/zpch-2019-1495

Okabe, N., & Kyoyama, H. (2001). 2,3-Dihydroxybenzoic acid. *Acta Crystallographica Section E Structure Reports Online*, *57*(12), o1224–o1226. https://doi.org/10.1107/S1600536801018682

Piwowar, A. M., Lockyer, N. P., & Vickerman, J. C. (2009). Salt effects on ion formation in desorption mass spectrometry: An investigation into the role of alkali chlorides on peak suppression in time-of-flight-secondary ion mass spectrometry. *Analytical Chemistry*, *81*(3), 1040–1048. https://doi.org/10.1021/ac8020888

Postberg, F., Kempf, S., Schmidt, J., Brilliantov, N., Beinsen, A., Abel, B., et al. (2009). Sodium salts in E-ring ice grains from an ocean below the surface of Enceladus. *Nature*, *459*(7250), 1098–1101. https://doi.org/10.1038/nature08046

Postberg, F., Khawaja, N., Abel, B., Choblet, G., Glein, C. R., Gudipati, M. S., et al. (2018). Macromolecular organic compounds from the depths of Enceladus. *Nature*, *558*(7711), 564–568. https://doi.org/10.1038/s41586-018-0246-4

Remusat, L., Derenne, S., & Robert, F. (2005). New insight on aliphatic linkages in the macromolecular organic fraction of Orgueil and Murchison meteorites through ruthenium tetroxide oxidation. *Geochimica et Cosmochimica Acta*, *69*(17), 4377–4386. https://doi.org/10.1016/j.gca.2005.05.003

Reusch, N., Krein, V., Wollscheid, N., & Weitzel, K.-M. (2018). Distinction of structural isomers of benzenediamin and difluorobenzene by means of chirped femtosecond laser ionization mass spectrometry. *Zeitschrift für Physikalische Chemie*, *232*(5–6), 689–703. https://doi.org/10.1515/zpch-2017-1051

Roth, L., Saur, J., Retherford, K. D., Strobel, D. F., Feldman, P. D., McGrath, M. A., & Nimmo, F. (2014). Transient water vapor at Europa's South Pole. *Science*, *343*(6167), 171–174. https://doi.org/10.1126/science.1247051

Sanderink, A., Klenner, F., Zymak, I., Žabka, J., Postberg, F., Lebreton, J.-P., et al. (2023). OLYMPIA-LILBID: A new laboratory setup to calibrate spaceborne hypervelocity ice grain detectors using high-resolution mass spectrometry. *Analytical Chemistry*, *95*(7), 3621–3628. https://doi.org/10.1021/acs.analchem.2c04429

Sankaranarayanan, R., Valiveti, C., Dachineni, R., Kumar, D., Lick, T., & Bhat, G. (2019). Aspirin metabolites 2,3-DHBA and 2,5-DHBA inhibit cancer cell growth: Implications in colorectal cancer prevention. *Molecular Medicine Reports*, 20–34. https://doi.org/10.3892/mmr.2019.10822

Schenk, P. M., Clark, R. N., Howett, C. J. A., Verbiscer, A. J., Waite, J. H., & Dotson, R. (Eds.) (2018). *Enceladus and the icy moons of Saturn*. University of Arizona Press.

Scherer, S., Altwegg, K., Balsiger, H., Fischer, J., Jäckel, A., Korth, A., et al. (2006). A novel principle for an ion mirror design in time-of-flight mass spectrometry. *International Journal of Mass Spectrometry*, *251*(1), 73–81. https://doi.org/10.1016/j.ijms.2006.01.025

Schulze, J. A., Yilmaz, D. E., Cable, M. L., Malaska, M., Hofmann, A. E., Hodyss, R. P., et al. (2022). Effect of salts on the formation and hypervelocity-induced fragmentation of icy clusters with embedded amino acids. *ACS Earth and Space Chemistry*, *7*(1), 168–181. https://doi.org/10.1021/acsearthspacechem.2c00267

Spahn, F., Schmidt, J., Albers, N., Hörning, M., Makuch, M., Seiß, M., et al. (2006). Cassini dust measurements at Enceladus and implications for the origin of the E ring. *Science*, *311*(5766), 1416–1418. https://doi.org/10.1126/science.1121375

Sparks, W. B., Hand, K. P., McGrath, M. A., Bergeron, E., Cracraft, M., & Deustua, S. E. (2016). Probing for evidence of plumes on Europa with HST/STIS. *The Astrophysical Journal*, *829*(2), 121. https://doi.org/10.3847/0004-637X/829/2/121

Spencer, J. R., Pearl, J. C., Segura, M., Flasar, F. M., Mamoutkine, A., Romani, P., et al. (2006). Cassini encounters Enceladus: Background and the discovery of a south polar hot spot. *Science*, *311*(5766), 1401–1405. https://doi.org/10.1126/science.1121661

Srama, R., Ahrens, T. J., Altobelli, N., Auer, S., Bradley, J. G., Burton, M., et al. (2004). The Cassini Cosmic Dust Analyzer. *Space Science Reviews*, *114*(1–4), 465–518. https://doi.org/10.1007/s11214-004-1435-z

Summons, R. E., Albrecht, P., McDonald, G., & Moldowan, J. M. (2008). Molecular biosignatures. *Space Science Reviews*, *135*(1–4), 133–159. https://doi.org/10.1007/s11214-007-9256-5

Thiessenhusen, K.-U., Krüger, H., Spahn, F., & Grün, E. (2000). Dust grains around Jupiter—The observations of the Galileo dust detector. *Icarus*, *144*(1), 89–98. https://doi.org/10.1006/icar.1999.6277

Venturi, S., Tassi, F., Gould, I. R., Shock, E. L., Hartnett, H. E., Lorance, E. D., et al. (2017). Mineral-assisted production of benzene under hydrothermal conditions: Insights from experimental studies on C 6 cyclic hydrocarbons. *Journal of Volcanology and Geothermal Research*, *346*, 21–27. https://doi.org/10.1016/j.jvolgeores.2017.05.024

Waite, J. H., Combi, M. R., Ip, W.-H., Cravens, T. E., McNutt, R. L., Kasprzak, W., et al. (2006). Cassini Ion and Neutral Mass Spectrometer: Enceladus plume composition and structure. *Science*, *311*(5766), 1419–1422. https://doi.org/10.1126/science.1121290

Waite, J. H., Glein, C. R., Perryman, R. S., Teolis, B. D., Magee, B. A., Miller, G., et al. (2017). Cassini finds molecular hydrogen in the Enceladus plume: Evidence for hydrothermal processes. *Science*, *356*(6334), 155–159. https://doi.org/10.1126/science.aai8703

Widhalm, J. R., & Dudareva, N. (2015). A familiar ring to it: Biosynthesis of plant benzoic acids. *Molecular Plant*, *8*(1), 83–97. https://doi.org/10.1016/j.molp.2014.12.001

Wiederschein, F., Vöhringer-Martinez, E., Beinsen, A., Postberg, F., Schmidt, J., Srama, R., et al. (2015). Charge separation and isolation in strong water droplet impacts. *Physical Chemistry Chemical Physics*, *17*(10), 6858–6864. https://doi.org/10.1039/C4CP05618C

Yamagaki, T., Takeuchi, M., Watanabe, T., Sugahara, K., & Takeuchi, T. (2016). Mechanism for odd-electron anion generation of dihydroxybenzoic acid isomers in matrix-assisted laser desorption/ionization mass spectrometry with density functional theory calculations. *Rapid Communications in Mass Spectrometry*, *30*(24), 2650–2654. https://doi.org/10.1002/rcm.7761